URSI GASS 2023, Sapporo, Japan, 19 - 26 August 2023

Measurements and Analysis of Angular Channel Characteristics in Substation Scenarios for Power IoT

Tao Zhou*(1), Yiteng Lin(1), and Liu Liu(1)
(1) School of Electronics and Information Engineering, Beijing Jiaotong University, Beijing 100044, P.R.China
e-mail: taozhou@bjtu.edu.cn; 20120066@bjtu.edu.cn; liuliu@bjtu.edu.cn

Abstract

To support the implementation of wireless communication technologies in power Internet of Things (PIoT), channel measurements and characterization for typical electrical scenarios should be investigated. In this work, we present a phased array antenna-based channel sounder and propose a multipath components (MPCs) extraction algorithm for directional channel measurements. The field tests are conducted in a 110 kV GIS room and a semi-indoor 110 kV substation to measure the angular channel characteristics, including the power angle delay profile and the angle spread of departure and arrival. These results can contribute to the planning and optimization of PIoT wireless communication system.

1 Introduction

In recent years, the integration of advanced information and communication technologies (ICT) and traditional industry has become a research hotspot, such as the power Internet of Things (PIoT) [1, 2]. In the power system, the application of PIoT in the transformation segment (e.g., substations) has received disproportionate attention and benefits, owing to its extremely harsh environment. Wireless communication networks are the core of the PIoT, which ensures efficient and reliable data transmission. Hence, an in-depth knowledge of the wireless channels of the working environment is a prerequisite for the deployment of PIoT in substation scenarios [3].

Up to now, there were relatively few channel measurements and characterizations conducted for substation scenarios, especially the directional measurements. Most of previous studies focused on large-scale and small-scale characteristics in the power domain and delay domain of substation channels, such as the path loss, shadow fading, power delay profile and root-mean-square (RMS) delay spread [4, 5]. In [6], the angular channel parameters like RMS angle spread of arrival were measured with a virtual rectangular antenna array in an outdoor 220 kV high-voltage substation at 28 GHz. However, some other significant characteristics to characterize the angle dispersion are still lacking, and the channels of indoor and semi-indoor substations still lack analysis in the angle domain.

In this work, a directional channel sounder is presented and a MPCs extraction algorithm is proposed. The wideband directional channel measurements are conducted in two typical substation scenarios at 3.35 GHz and several angular channel characteristics are extracted and analyzed.

2 Channel Measurements in Substations

2.1 Directional Channel Sounder

To achieve double directional wideband channel measurement, we designed a channel sounder equipped with phased array antennas, as shown in Fig. 1. The measurement system consists of two parts, including the transmitter (TX) and the receiver (RX). The TX uses a baseband signal generator (BSG) and a vector signal generator (VSG) which can generate up to 150 MHz bandwidth excitation signal. An orthogonal frequency division multiplexing (OFDM) signal is chosen as the excitation signal. The RX adopts a radio frequency unit for signal amplification and mixing, and uses a data acquisition card and solid state disk (SSD) to collect and store the raw measurement data. The phased array antennas with 16 by 4 antenna elements are operated at both TX and RX side, which can work at 3.3-3.5 GHz and support horizontal narrow-beam steering. Note that the Rubidium clock are used to ensure the consistency of reference clocks of all equipment.

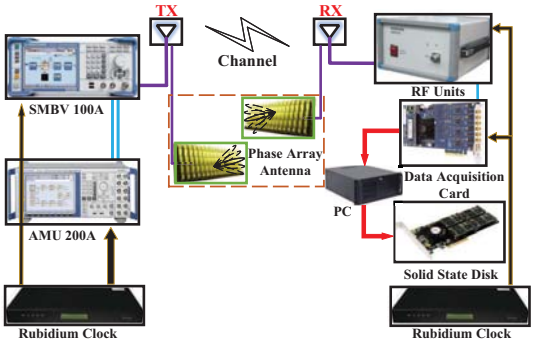

Figure 1. Channel sounder for directional measurements.

The directional channel measurements rely on beam sweeping of TX/RX antenna, which is switched from $-45°$ to $+45°$ in $5°$ steps and a total of 19 directions of the TX/RX beam are detected. For each TX beam, 19 beam pairs can

be received. Thus, a total of 19 by 19 beam pairs can be measured during a full-sweep covering 90° azimuth of both TX and RX. Besides, in order to guarantee the phase continuity of different beams and avoid the uncertainty of absolute delay, we collect the data continuously and store them intermittently.

2.2 Data Post Processing

In order to extract channel information from the raw measurement data, we employ the widely used frequency-domain method to obtain the channel impulse responses (CIRs). According to the extracted CIRs for all TX-RX beam pairs, the power angle delay profile (PADP) consists of the angle of departure (AOD) ϕ_{TX}, the angle of arrival (AOA) ϕ_{RX} and the delay τ can be estimated as [7]

$$PADP(\phi_{\mathrm{TX}},\phi_{\mathrm{RX}},\tau) = \left|\mathscr{F}^{-1}\left\{H(\phi_{\mathrm{TX}},\phi_{\mathrm{RX}},f)\cdot G^{*}(f)/|G(f)|^{2}\right\}\right|^{2} \quad (1)$$

where $\phi_{\mathrm{TX/RX}} \in [-45^{\circ}, 45^{\circ}]$, $\mathscr{F}^{-1}$ indicates inverse Fourier transform, $H(\phi_{\mathrm{TX}},\phi_{\mathrm{RX}},f)$ indicates the channel frequency response for the TX and RX beams with the azimuth angles ϕ_{TX} and ϕ_{RX}, $G(f)$ donates the system response and $(\cdot)^{*}$ donates the conjugation operation.

Since the measured CIRs contain both invalid MPCs and noise components, a directional MPCs extraction algorithm is applied to the PADPs, which procedure is described in Algorithm 1. Note that a peak search method with dynamic noise threshold is utilized. Firstly, we apply the peak search to each PADP in the delay domain to obtain the peaks with power greater than the noise threshold N_{th}. Then the peak search are performed in the angle domain for both TX and RX beams to eliminate the invalid MPCs caused by beam overlap. Subsequently, we filter out the ghost MPCs due to the beams side-lobes. In each delay bin, the local strongest peak within 20 dB of the global strongest MPC is accepted as a MPC and other peaks are further processed. Since the main lobe is found to be at least 10 dB stronger than the side-lobes, we only accept the peaks within 10 dB of the local strongest MPC at each delay. Finally, the peaks that have powers within 20 dB of the local strongest MPC and with both AOD and AOA different from the local strongest MPC are retained. Therefore, the dynamic range of per resolvable delay bin is limited to 20 dB in this algorithm.

2.3 Measurement Campaigns

We performed a series of directional wideband channel measurements in two typical substations, e.g., an 110 kV GIS room and a semi-indoor 110 kV substation. The measurements were conducted in 3.35 GHz carrier frequency and 100 MHz bandwidth. As shown in Fig. 2, two propagation conditions including line of sight (LOS) and non-line of sight (NLOS) were measured in the semi-indoor 110 kV substation, while the 110 kV GIS room was only measured for the LOS case. In the GIS room, there are various mental equipment housed in the central area. While in the semi-indoor substation, the main reflectors are upright isolation-switch posts with dispersed distribution.

Algorithm 1: Directional MPCs Extraction

Input: $PADP(\phi_{\mathrm{TX}},\phi_{\mathrm{RX}},\tau), N_{\mathrm{th}}$
Output: MPCs list

```
Initialize MPCs list;
Perform peak research on PADP(τ);
Perform peak research on PADP(φ_TX) and PADP(φ_RX) respectively;
Store peaks p(φ, τ), φ = [φ_TX, φ_RX];
p_max ← max p(φ, τ);
for all τ do
    τ_n ← τ;
    if p(φ, τ_n) is not empty then
        p_{τ_n,max} ← max_φ p(φ, τ_n), φ_max ← arg max_φ p(φ, τ_n);
        if p_{τ_n,max} ≥ p_max/100 then
            for all p(φ, τ_n) do
                if p(φ, τ_n) > p_{τ_n,max}/10 then
                    Add p(φ, τ_n) to the MPCs list;
                end
                else if (p(φ, τ_n) > p_max/100) &
                (φ_TX ≠ φ_TX,max) & (φ_RX ≠ φ_RX,max) then
                    Add p(φ, τ_n) to the MPCs list;
                end
            end
        end
    end
end
```

In the field measurement, both the TX and RX antennas were fixed at both ends of the room, and measured the front 90° sectors. Note that the RX antenna was tilted to the right by about 30° in the GIS room, and the TX antenna was parallel to the wall behind. In the semi-indoor substation, the TX and RX antennas were placed in parallel. In the measurement plan, the TX position is marked with a red square and the RX positions for the LOS and NLOS measurements are identified by red and blue squares, respectively.

3 Angular Channel Characterization

With the data post processing, the angular channel characteristics of the measurement scenarios can be visualized and analyzed. Fig. 3 depicts the received power for all TX and RX beam pairs measured in the substations, including the LOS case for the GIS room and the LOS and NLOS case for the semi-indoor substation. From Fig. 3(a) and Fig. 3(b), the LOS components are observed at RX angle x and TX angle y with $(-30^{\circ},\ 5^{\circ})$ and $(5^{\circ},\ -5^{\circ})$ respectively, which are practically consistent with the actual TX and RX positions in two substation scenarios. In Fig. 3(c), a dominant

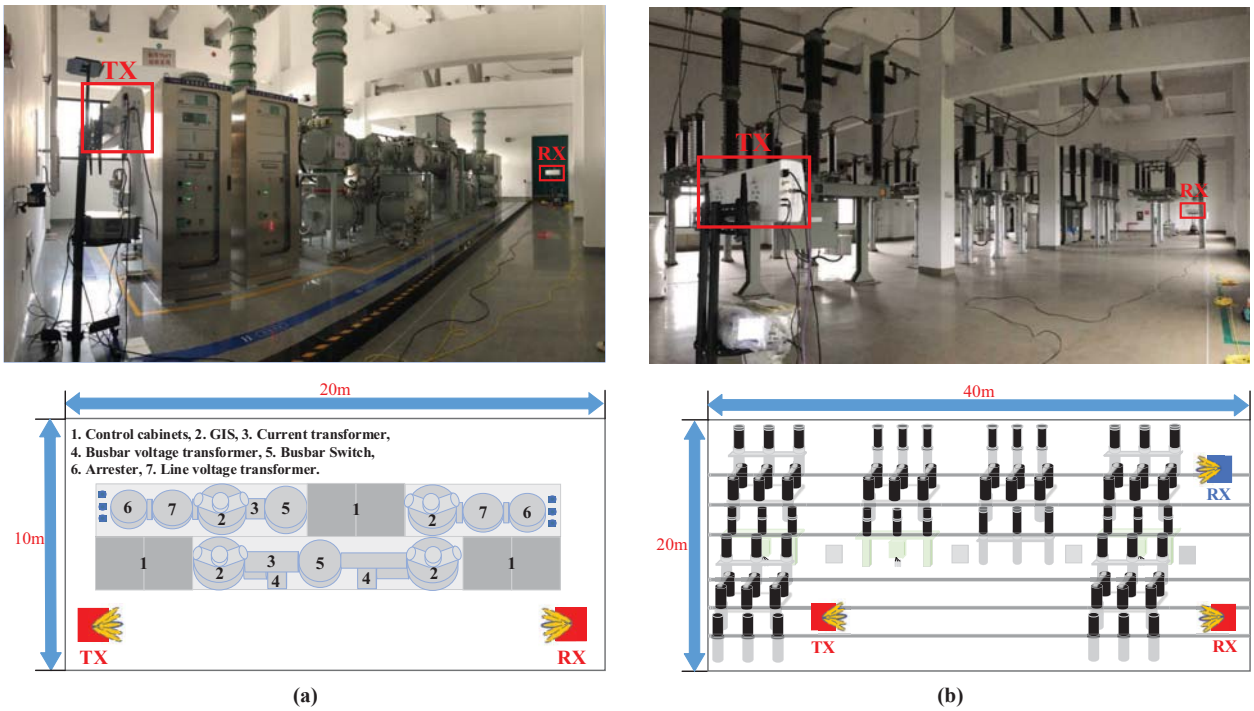

Figure 2. Measurement scenarios and layout in two substations. (a) 110 kV GIS room. (b) Semi-indoor 110 kV substation.

MPC with the strongest power is observed at $(-15°, 20°)$ in the NLOS case, which is reflected from the wall on the left side of RX. In addition, the received power in the NLOS case is 10 dB less compared to the LOS case.

Fig. 4 shows the results of PADP with valid MPCs extraction. It is observed that the MPCs in each delay bin with different AOAs and AODs are identified. As can be seen from Fig. 4(a) and Fig. 4(b), the number of MPCs are similar in the LOS case for the GIS room and the semi-indoor substation, while the latter exists MPCs with stronger power and smaller delay than the former. This can be explained by the presence of a continuous of electrical equipment between TX and RX in the GIS room, which causes the propagating waves to undergo more reflections. With regard to the NLOS case, it can be observed from Fig. 4(c) that more MPCs are measured in almost all directions. Notably, almost no dominant MPCs with higher power are observed when the AOD exceeds $-20°$, which implies that the posts located on the left side of the TX largely prevent the propagation of the MPCs.

To quantify the angle dispersion, the RMS angle spread (AS) is commonly estimated, involving the RMS angle spread of departure (ASD) and RMS angle spread of arrival (ASA), which can be calculated according to the joint power angular spectrum (PAS):

$$AS = \sqrt{\frac{\int PAS(\phi)\,\phi^2 d\phi}{\int PAS(\phi)\,d\phi} - \left(\frac{\int PAS(\phi)\,\phi d\phi}{\int PAS(\phi)\,d\phi}\right)^2} \quad (2)$$

where PAS for joint TX beam and RX beam can be simply estimated based PADP, expressed as

$$PAS(\phi_{\mathrm{TX}}, \phi_{\mathrm{RX}}) = \sum_{\tau} PADP(\phi_{\mathrm{TX}}, \phi_{\mathrm{RX}}, \tau) \quad (3)$$

Based on the PASs for AOD and AOA, the calculation results of the RMS AS are obtained and listed in Table I. The RMS ASD and ASA are calculated as 10.4° and 7.82° in the GIS room, and the values are respectively 9.58° and 8.43° for the LOS case and 13.9° and 21.1° for the NLOS case in the semi-indoor substation. It has been published in [6] that the average values of RMS ASA are 30.9° and 28.8° for the LOS and NLOS measurements in the 220 kV outdoor substation. Therefore, it can be inferred that the angle dispersion of the indoor substation is weaker than that of the outdoor substation.

Table 1. Comparison of RMS AS results in different substation scenarios

Scenario	GIS room	Semi-indoor substation		Outdoor substation [6]	
Case	LOS	LOS	NLOS	LOS	NLOS
RMS ASD (°)	10.4	9.58	13.9	-	-
RMS ASA (°)	7.82	8.43	21.1	30.9	28.8

4 Conclusion

In this work, a phase array antenna based channel sounder has been designed, including the measurement system and the corresponding directional MPCs extraction algorithm. The directional channel measurements have been conducted in the 110 kV GIS room and semi-indoor 110 kV substa-

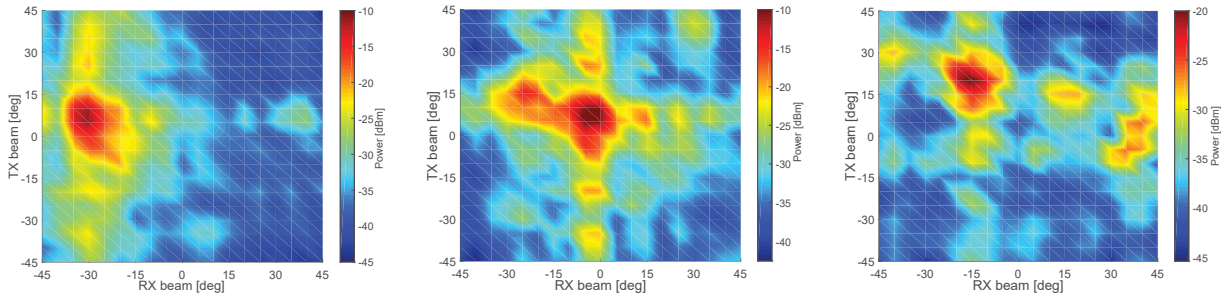

Figure 3. Received power for TX-RX beam pairs in the measured substation scenarios. (a) 110 kV GIS room (LOS case). (b) Semi-indoor 110 kV substation (LOS case). (c) Semi-indoor 110 kV substation (NLOS case).

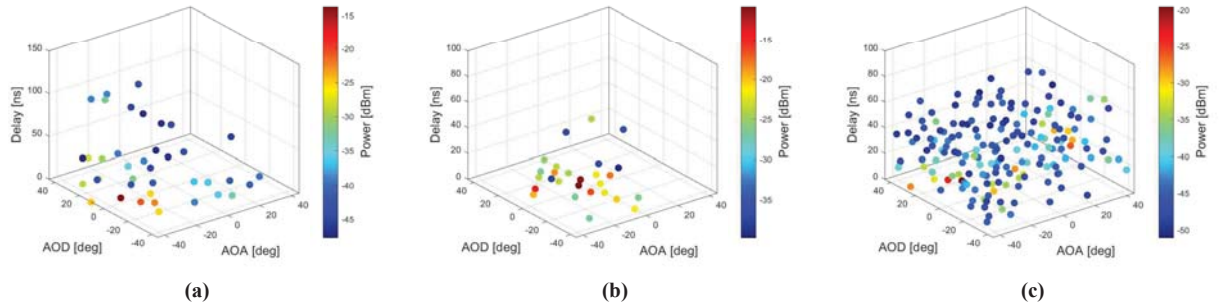

Figure 4. PADP results in the measured substation scenarios. (a) 110 kV GIS room (LOS case). (b) Semi-indoor 110 kV substation (LOS case). (c) Semi-indoor 110 kV substation (NLOS case).

tion for LOS and NLOS conditions. The directional multipath propagation characteristics of substation channels have been characterized in terms of received power and PADP. Moreover, the results of RMS ASD and RMS ASA have been also presented. These results are significant for the planning and optimization of PIoT in substation scenarios.

Acknowledgements

This work was supported by the Science & Technology Project of State Grid Corporation of China (Research on Reliability Technologies for Transformer Substation Wireless Networks in Complex Electromagnetic Environments, 5500-202055070A-0-0-00), the National Natural Science Foundation of China under Grant 62071031, the Beijing Natural Science Foundation under Grants L212030 and 4212006.

References

[1] L. Ma, W. Li, Y. Hou, W. Zhan, R. Yang, W. Jia, Y. Qiu, “Application of Wireless Communication Technology in Ubiquitous Power Internet of Things,” in *Proc. IEEE Int. Conf. Comput. Commun. Eng. Technol.*, Beijing, China, 2020, pp. 267-271.

[2] B. Chen, L. Chen, Y. Tan and X. Kuang, “Investigations on Communication and Management Techniques for Electric Internet of Things Applications in Smart Grid,” in *Proc. 2021 China International Conference on Electricity Distribution (CICED)*, 2021, pp. 515-518.

[3] T. Zhou, H. Zhang, B. Ai, C. Xue and L. Liu, “Deep-learning based spatial-temporal channel prediction for smart high-speed railway communication networks," *IEEE Trans. Wireless Commun.*, vol. 21, no. 7, pp. 5333-5345, 2022.

[4] R. M. Sandoval, A. Garcia-Sanchez, J. Molina-Garcia-Pardo, F. Garcia-Sanchez and J. Garcia-Haro, “Radio-Channel Characterization of Smart Grid Substations in the 2.4-GHz ISM Band,” *IEEE Trans. Wirel. Commun.*, vol. 16, no. 2, pp. 1294-1307, 2017.

[5] Q. Li, H. Zhang, T. Zheng, X. Wang and Y. Lv, “Maximum inner product method for extracting the path-loss parameters in primary transformer substations,” *China Commun.*, vol. 16, no. 4, pp. 120-129, 2019.

[6] Z. Fu, H. Cui, S. Geng and X. Zhao, “5G Millimeter Wave Channel Modeling and Simulations for a High-Voltage Substation,” in *Proc. IEEE Sustain. Power Energy Conf.*, Beijing, China, 2019, pp. 1822-1826.

[7] C. U. Bas, R. wang, S. Sangodoyin, D. Psychoudakis, T. Henige, R. Monroe, J. Park, J. Zhang, A. F. Molish, “Real-Time Millimeter-Wave MIMO Channel Sounder for Dynamic Directional Measurements,” *IEEE Trans. Veh. Technol.*, vol. 68, no. 9, pp. 8775-8789, 2019.